



## Complement system is activated in acute inflammatory response to environmental particulates in the lungs

Kerui Zhang<sup>a</sup>, Akiko Honda<sup>a,\*</sup>, Tomoya Sagawa<sup>b,c</sup>, Natsuko Miyasaka<sup>b</sup>, Binyang Qiu<sup>a</sup>, Raga Ishikawa<sup>b</sup>, Tomoaki Okuda<sup>d</sup>, Takayuki Kameda<sup>e</sup>, Kaori Sadakane<sup>f</sup>, Takamichi Ichinose<sup>b,f</sup>, Hirohisa Takano<sup>b,g,h,\*\*</sup>

<sup>a</sup> Graduate School of Engineering, Kyoto University, Kyoto, Japan

<sup>b</sup> Graduate School of Global Environmental Studies, Kyoto University, Kyoto, Japan

<sup>c</sup> Inflammation and Immunology, Graduate School of Medical Science, Kyoto Prefectural University of Medicine, Kyoto, Japan

<sup>d</sup> Department of Applied Chemistry, Faculty of Science and Technology, Keio University, Kanagawa, Japan

<sup>e</sup> Graduate School of Energy Science, Kyoto University, Kyoto, Japan

<sup>f</sup> Department of Health Sciences, Oita University of Nursing and Health Sciences, Oita, Japan

<sup>g</sup> Institute for International Academic Research, Kyoto University of Advanced Science, Kyoto, Japan

<sup>h</sup> Research Institute for Coexistence and Health Science, Kyoto University of Advanced Science, Kyoto, Japan

### ARTICLE INFO

Edited by : Professor Bing Yan

#### Keywords:

Particulate matter

Complement component C5 activation

C5aR1

C5b-9

Inflammatory response

Lung disease

### ABSTRACT

Short-term exposure (typically ranging from a few hours to 7 days) to particulate matter (PM) elicits acute inflammatory responses with significant activation of complement component C5. However, the relationship between PM-induced complement system activation, acute inflammation, and the contributing factors remains unclear. In this study, we aimed to investigate the intensity of acute inflammatory responses, as well as the activation levels of complement C5 and its related products, C5aR1 and C5b-9, following exposure to different types of PM. Acute inflammatory responses and complement activation were assessed in mice intratracheally administered four types of PM: titanium dioxide (TiO<sub>2</sub>), diesel exhaust particles (DEP), Asian sand dust (ASD), and ambient PM with an aerodynamic diameter  $\leq 2.5 \mu\text{m}$  (PM<sub>2.5</sub>). Complement system and inflammatory markers were evaluated by analyzing increased C5 protein levels, C5b-9 deposition, and C5aR1 expression. Additionally, dark-field microscopy and Raman microscopy were used to detect PM components adjacent to infiltrating neutrophils, and elemental composition was quantified using ICP-MS and EDXRF. ASD, DEP, and PM<sub>2.5</sub> exposure significantly increased C5b-9 deposition in lung tissues. All PM-exposed groups exhibited substantial upregulation of C5aR1 expression, primarily in neutrophils. Raman spectroscopic analysis revealed Si, K, Mg, Al, and Fe adjacent to infiltrating neutrophils in ASD-exposed lungs. Furthermore, elemental analysis identified Si, Mg, Al, and K as the most potent contributors to complement activation and inflammatory responses. Of the four types of PM, ASD induced the most severe acute inflammatory response and complement system activation. Therefore, ASD-induced complement system activation, driven at least partly by its mineral components, may play a critical role in neutrophil activation and acute pulmonary inflammation. These findings highlight the differential impact of PM types on complement system activation and underscore the importance of PM composition in the evaluation of air pollution-related health risks, particularly acute pulmonary inflammation.

### 1. Introduction

Asia has high levels of air pollution caused by rapid growth in

industrialization, urbanization, and motor vehicle transportation (Atkinson et al., 2012). This increase in air pollution is also attributed to desertification and desert sandstorms, accompanied by air pollutant

\* Correspondence to: Department of Environmental Engineering, Graduate School of Engineering, Kyoto University, C Cluster, Kyoto-Daigaku-Katsura, Nishikyoku, Kyoto 615-8540, Japan.

\*\* Corresponding author at: Institute for International Academic Research, Kyoto University of Advanced Science, Kyoto, Japan.

E-mail addresses: [akko@health.env.kyoto-u.ac.jp](mailto:akko@health.env.kyoto-u.ac.jp) (A. Honda), [takano.hirohisa@kuas.ac.jp](mailto:takano.hirohisa@kuas.ac.jp) (H. Takano).

<https://doi.org/10.1016/j.ecoenv.2025.118259>

Received 10 October 2024; Received in revised form 1 April 2025; Accepted 27 April 2025

Available online 1 May 2025

0147-6513/© 2025 The Authors. Published by Elsevier Inc. This is an open access article under the CC BY-NC license (<http://creativecommons.org/licenses/by-nc/4.0/>).

particulate matter (PM) that can be transported over long distances (Zhang et al., 2017). Consequently, the impact of air pollution on human health is drawing increasing public attention. Inhalable PM originate from both anthropogenic activities (e.g., combustion, industrial production) and natural sources (e.g., dust, volcanic activity) (Yang et al., 2020), thereby forming a complex mixture of particles with diverse compositions and physical and chemical properties (Falcon-Rodriguez et al., 2016). Accumulating epidemiological and toxicological studies have identified certain chemical components, such as silicon (Benmerzoug et al., 2018; Wang et al., 2020), endotoxin (He et al., 2017), carbonaceous particles (Yang et al., 2021), and metals (Chen et al., 2021; Rosa et al., 2016; Chowdhury et al., 2019), as key contributors to the toxicity of PMs. Therefore, different types of PM can induce varying levels of lung inflammation.

The representative PM types, including titanium dioxide (TiO<sub>2</sub>), diesel exhaust particles (DEP), Asian sand dust (ASD), and ambient PM with an aerodynamic diameter  $\leq 2.5 \mu\text{m}$  (PM<sub>2.5</sub>), increase the disease burden on respiratory health. Epidemiologically, the presence of metals is one of the factors that induces the respiratory effects of PM<sub>2.5</sub> (Ghobakhloo et al., 2024, 2025). Although TiO<sub>2</sub> is not considered a traditional inhalable PM, it can be absorbed through both inhalation and ingestion (Braakhuis et al., 2021). Owing to its extremely small particle size, TiO<sub>2</sub> may pose more severe risks and impacts on human health. Current experimental studies have consistently shown a correlation between exposure to TiO<sub>2</sub> (Baisch et al., 2014), DEP (Tao et al., 2021), ASD (Naota et al., 2013; He et al., 2016), and PM<sub>2.5</sub> (Lin et al., 2022; Zhao et al., 2022; Zhang et al., 2020) and acute inflammatory responses of the respiratory system. For example, the intratracheal instillation of high-dose TiO<sub>2</sub> for 24 h significantly increased alveolar macrophage and neutrophil counts in bronchoalveolar lavage fluid (BALF) (Baisch et al., 2014). Similarly, DEP instillation induced considerable pulmonary inflammation characterized by elevated neutrophils counts and levels of inflammatory cytokines such as TNF- $\alpha$  in BALF, accompanied by histological signs of tissue inflammation (Tao et al., 2021). Inflammatory responses to ASD included macrophage and neutrophil activation and inflammatory cell infiltration around particles (Naota et al., 2013; He et al., 2016). Moreover, short-term PM<sub>2.5</sub> exposure caused dose-dependent pro-inflammatory cytokine release and significant inflammatory cell infiltration (Lin et al., 2022; Zhao et al., 2022; Zhang et al., 2020). These findings demonstrate that macrophage and neutrophil activation, as well as cytokine release in the lung, are the most common PM-induced characteristics. However, differences in the potential mechanisms underlying the inflammatory response induced by various PM have not been clarified.

As the front line of immune defense, the complement system serves as both an immune sensor and activator. Pattern recognition receptors (PRRs) in this system, such as C1q, mannose-binding lectin (MBL), and ficolin, respond to exogenous and endogenous stimulation, consequently activating three separate downstream pathways: the classical pathway, triggered by antibodies binding to pathogens; the lectin pathway, activated by specific sugar patterns on microbial surfaces recognized by lectins such as MBL; and the alternative pathway, which is continuously active at low levels and can be spontaneously triggered on microbial surfaces. These pathways enable the identification and elimination of pathogens and toxins in the immune system (Dunkelberger and Song, 2010). Although each pathway is activated by distinct PRRs (Hovland et al., 2015), they all converge on the complement component C5, resulting in the generation of the pro-inflammatory anaphylatoxin C5a and membrane attack complexes (MAC). The complement system is not only involved in innate immune responses but also interacts with and influences acquired immune responses (Reis et al., 2019). C5, a pivotal component of the complement cascade, regulates the function of macrophages (Hu et al., 2014), neutrophils (Ehrnthaller et al., 2021), and dendritic cells (Antonioni et al., 2020). It also contributes to the onset and progression of many lung diseases, such as acute lung injury (Kalbitz et al., 2016), pneumonia (Müller-Redetzky et al., 2020), and

bronchial asthma (Hu et al., 2017; Yang et al., 2019). In addition, the complement system is activated during PM exposure (Choi et al., 2021; Jin et al., 2019; Husain et al., 2015). TNF- $\alpha$ , a critical pro-inflammatory cytokine in PM-induced inflammation, is produced by various immune cells following the activation of complement component C5 (Wang et al., 2015). However, the modulation of C5 levels and responses of its related components by PM, as well as the specific components contributing to complement activation remain unclear. Thus, the deleterious effects of PM on the respiratory system and the pathophysiological consequences of complement component C5 activation in lung diseases necessitate further investigation on the modulation of C5 levels and related component responses by PM.

Raman spectroscopy is advantageous for identifying materials using spectroscopic fingerprints generated by laser irradiation without staining. Its application in biological fields has rapidly increased, owing to cell and spectral tissue imaging. In our previous studies, we either combined hematoxylin and eosin (HE) or immunohistochemistry (IHC) (Akaji et al., 2022; Sagawa et al., 2021) staining with Raman spectral acquisition on identical tissue slides. Additionally, dark-field microscopy was used to screen areas where the presence of TiO<sub>2</sub> was suspected. This technique demonstrates the relationships between PM and pathological, physiological, and molecular changes. However, it has not been applied to particles other than TiO<sub>2</sub>. The combination of dark-field microscopy with Raman spectroscopy is expected to elucidate the location of various particles in the lungs. This will facilitate further investigation of the relationship between these particles and their biological effects, as well as elucidation of the mechanisms underlying their pathogenesis.

In the present study, we aimed to clarify the relationship between PM-induced acute inflammatory responses and complement system activation. Additionally, we aimed to identify the components contributing to complement activation with spatial location information in the lungs. Our findings provide evidence of the detrimental effects of air pollutant exposure on pulmonary inflammation, which could be valuable for the evaluation of PM-induced acute pulmonary inflammation.

## 2. Materials and methods

### 2.1. Animals

Male ICR mice (8 weeks old) were purchased from Charles River Japan Inc. (Kanagawa, Japan). The mice were acclimated for one week and maintained at 23–25 °C and 50–70 % relative humidity under conventional conditions with a 12 h light/dark cycle. They were fed a CE-2 commercial diet (CLEA Japan, Inc., Tokyo, Japan) and provided with water *ad libitum*. The mice were housed in plastic cages lined with soft wood chips. This study was conducted in accordance with the United States National Institutes of Health guidelines on the use of experimental animals and the Animal Research Reporting of in Vivo Experiments (ARRIVE) guidelines. In addition, the animal experiments were approved by the Animal Research Committee of Oita University of Nursing and Health Sciences (approval number: 20–88).

### 2.2. Preparation of particle samples

TiO<sub>2</sub> particles were provided by Sakai Chemical Industry Co., Ltd. (STR-100N; Osaka, Japan). Rutile TiO<sub>2</sub> particles with no chemical treatments and a primary particle size of 15 nm were used. DEP particles (National Institute for Environmental Studies, Tsukuba, Japan) were collected as previously described (Nakamura et al., 2012). Briefly, an 8-L diesel engine (Fujitani et al., 2009) (J08C; Hino Motors, Tokyo, Japan) that was not fitted with after-treatment devices was powered under steady-state conditions (speed = 2000 rpm; engine torque = 0 Nm; diesel fuel = JIS No. 2) for 5 h. Particles were electrostatically (-27 kV) collected at approximately 10 m from the engine onto dichloromethane-washed gold discs at a flow rate of 20 L/min using an

SSPM-100 sampler (Shimadzu, Kyoto, Japan). ASD particles (CRM No.30) were obtained from the National Institute for Environmental Studies. PM<sub>2.5</sub> particles were collected from an urban residential area approximately 15 km south-southwest of the center of Tokyo, 4 km from the nearest expressway, and 10 km from a dense industrial area. Aerosol sampling was conducted as previously described (Honda et al., 2021) on the rooftop of a 22 m high building at Keio University, Yokohama, Japan, between January and February 2018. TiO<sub>2</sub>, DEP, ASD, and PM<sub>2.5</sub> particles were suspended in PBS and subjected to ultrasonication for 3 min at  $21 \pm 1$  kHz on ice (UD-100; TomySeiko, Tokyo, Japan).

### 2.3. Administration of particle samples

The ICR mice were divided into thirteen groups according to treatment: PBS only (n = 8); TiO<sub>2</sub> particles (n = 8), DEP (n = 8), ASD (n = 8), or PM<sub>2.5</sub> (n = 8) at doses of 50, 200, and 500  $\mu\text{g}/\text{mouse}$ . Dose selection was conducted as previously described (Yoshida et al., 2009). Briefly, 50  $\mu\text{g}$  of particle samples deposited into the lung of a single mouse were approximately 3 times the amounts in the Japanese national air quality standard for suspended PM (0.1  $\text{mg}/\text{m}^3$ ) accumulated in the lungs of a mouse/day (He et al., 2016; Schwarte et al., 2000).

Mice were sensitized through the intratracheal instillation of different doses of TiO<sub>2</sub>, DEP, ASD, and PM<sub>2.5</sub> in a 100  $\mu\text{L}$  PBS solution (Takara Bio, Kusatsu, Japan). An equal volume of PBS was administered to the control group. The mice were subjected to deep anesthesia via intraperitoneal injection of 0.2 mL (1.77 mg / 27 mg / mouse) of a mixture of pentobarbital sodium (Kyoritsu, Osaka, Japan) and medetomidine hydrochloride (Zenoaq, Fukushima, Japan) and euthanized 24 h after a single exposure to TiO<sub>2</sub>, DEP, ASD, or PM<sub>2.5</sub>. Samples were then collected for analysis.

### 2.4. Analysis of inflammatory cells in bronchoalveolar lavage fluid (BALF)

The lungs from five mice in each group were used to assess the accumulation of inflammatory cells in the BALF. After euthanasia, the lungs were washed thrice with 1.2 mL of 37 °C saline. The lavage fluid was harvested through gentle aspiration. The three lavage fluids were combined, preserved in a plastic tube, cooled to 4 °C, and centrifuged at 200 g  $\times$  g for 10 min. The immune cell count in the cell pellet was assessed using Turk's solution in a hemocytometer chamber.

After the cells were stained with Diff-Quik (Sysmex Co., Kobe, Japan), at least 500 cells were counted under a microscope for further classification and counting based on morphological criteria.

### 2.5. Quantitation of TNF- $\alpha$ in BALF and C5 in BALF and serum

Commercially available ELISA kits were used to quantify TNF- $\alpha$  (MTA00B; R&D systems, Minneapolis, MN, USA) and C5 (ab264609; Abcam, Cambridge, UK) in BALF and serum according to the manufacturers' instructions. Serum sampling was performed as previously described (Sadakane et al., 2022). In brief, serum samples were prepared from blood collected via cardiac puncture using a blood collection tube (CJ-2AS; Terumo Co., Tokyo, Japan) after the blood was centrifuged at 3000  $\times$  g for 10 min at room temperature.

### 2.6. IHC and triple IHC

Three mice from each group were evaluated using IHC. The lungs were collected, fixed in 4 % paraformaldehyde, and embedded in paraffin.

Immunohistochemical staining of C5aR1, C5b-9, Ly6G, F4/80, and CD11c was performed on paraffin-embedded sections. Lung 5  $\mu\text{m}$  thick) were dewaxed and rehydrated with an alcohol gradient and PBS. Endogenous peroxidases were blocked with 3 % H<sub>2</sub>O<sub>2</sub> in water for 5 min. Slides were subjected to heat-mediated antigen retrieval immersed in

citrate buffer (pH 6.0; Diagnostic BioSystems, CA, USA) for 15 min at 80 – 100 °C.

Nonspecific binding was blocked using Blocking One Histo (06349–64; Nacalai Tesque CO., Kyoto, Japan) for 10 min. For immunostaining, sections were incubated with C5aR1 (1:200, Rat, ab117579; Abcam), C5b-9 (1:800, Rabbit, ab55811; Abcam), Ly6G (1:400, Rat, 127601; Bio Legend, San Diego, CA, USA), F4/80 (1:100, Rat, MCA497G; Bio-Rad, Hercules, CA, USA), or CD11c (1:200, Rabbit, D1V9Y; Cell Signaling Technology, Danvers, MA, USA) primary antibodies overnight at 4 °C. Chromogenic detection was performed using 3-amino-9-ethylcarbazole (AEC) staining according to the manufacturer's instructions. Hematoxylin was used for counterstaining. Normal rabbit and rat IgGs were used as controls for IHC.

Triple IHC was performed as follows: After completion of the IHC staining for the previous target, the mounting medium was removed using xylene, followed by the elimination of AEC through a graded ethanol series. Subsequently, the slides were treated with citrate buffer at 80–100 °C for 15 min to remove nuclear staining and dissociate the primary antibody from the sample. Finally, the IHC staining procedure described in 2.6 was repeated for the subsequent target.

Pathological analysis of the lungs was performed using a KEYENCE fluorescence microscope (BZ-X800; KEYENCE, Osaka, Japan). The positivity (total number of positive pixels divided by total number of pixels in the observation area) of C5b-9 and C5aR1 was assessed using the Aperio Image Scope software (12.4; Leica Biosystems, Richmond Hill, ON, Canada) at 20  $\times$  magnification (Morozan et al., 2023). We excluded background staining (image noise) from the analysis to fine-tune the algorithm. To this end, the algorithm was run on selected regions containing only background AEC staining. We adjusted the initial intensity threshold of weak positive (Upper Limit) of 180 stepwise downward to contrast with completely negative annotated areas. An intensity threshold of 40 was used as the lower limit for strong positive staining (Suppl. Figures 1 and 2). The right lungs of three mice were selected from each group, and five sites were selected per lung lobe for a total of  $3 \times 4 \times 5 = 60$  sites.

### 2.7. Raman spectroscopic and dark-field imaging in lung tissues of mice

Immunostained sections were observed using an Olympus BX-53 microscope with an oil-immersion dark-field condenser to visualize particle localization. The sections were decolorized as previously described (Sagawa et al., 2021; Tsujikawa et al., 2017) to remove artifacts from the Raman measurements. Briefly, the slides were immersed in xylene to remove the cover glass and mounting media, immersed in ethanol to decolorize the AEC, rehydrated in a serial dilution of ethanol, and subjected to citrate buffer to remove the antibodies and hematoxylin.

The Raman spectra were obtained using a LabRAM HR Evolution confocal Raman microscope (Horiba, Kyoto, Japan). This system was connected to an Olympus microscope equipped with 100 objectives (NA 0.9) and a 300 gr/mm grating. A laser with a wavelength of 532 nm was used as the light source to obtain the Raman scattering; the laser intensity used for the measurements was approximately 0.8–4 mW. For Raman imaging analysis, Raman spectra were collected in 0.5–1  $\mu\text{m}$  steps in the x- and y-directions, respectively. Labspec6 software (Horiba) was used for Raman spectral data acquisition, preprocessing, and analysis. Specifically, preprocessing such as spike signal removal, baseline correction, and noise smoothing via singular value decomposition were performed. Next, the classical least squares model was used for Raman imaging analysis. The KnowItAll® spectral library (Wiley, USA) was used to identify particle components.

### 2.8. Analysis of chemical and biochemical components in particles

TiO<sub>2</sub>, DEP, ASD, and PM<sub>2.5</sub> were characterized using energy dispersive X-ray fluorescence for Si, inductively coupled plasma mass

spectrometry for metals (e.g., Mg, Al, Ca, V, Mn, Fe, and Co), and high-performance liquid chromatography with fluorescence detection for polycyclic aromatic hydrocarbon (PAH) components. Chemical characterization was performed previously described (Okuda, 2013; Okuda et al., 2013, 2014). The amount of endotoxin and glucan was calculated as a concentration per mg. Endotoxin levels were measured using a PyroColor-MP: Chromogenic Diazo-coupling Kit (Associates of Cape Cod. Inc., East Falmouth, MA, USA) and Pyrochrome with Glucashield Buffer (Seikagaku Corp., Tokyo, Japan). Contrastingly, the  $\beta$ -glucan content was measured using the GlucateLL Kit (Associates of Cape Cod. Inc.) as previously reported (Spaan et al., 2008) and according to the manufacturer's instructions, with some modifications. Briefly, the particle samples were suspended in water containing 0.05 % Tween for 1 h. The supernatants were recovered before LPS and  $\beta$ -glucan concentrations were measured through endpoint colorimetry.

## 2.9. Statistical analysis

Data are expressed as the mean  $\pm$  standard error of the mean (SEM). Statistical significance was determined through Dunnett's one-way analysis of variance (ANOVA). For correlation analysis, Pearson's correlation coefficient (two-tailed) was used to assess the relationship between TiO<sub>2</sub>, DEP, ASD, and PM2.5 components and the variations in the mean values of neutrophils, TNF- $\alpha$ , C5, C5aR1, and C5b-9, using SPSS

Statistics 29 (IBM Corp., Armonk, NY, USA.). The results of the correlation analysis were visualized as a heatmap, and other statistical analyses were performed using GraphPad Prism 9.4.1 (GraphPad Software Inc., San Diego, CA, USA). Differences among groups were determined as statistically significant at  $p < 0.05$ . The symbols \*, \*\*, \*\*\*, and \*\*\*\* indicate P values below 0.05, 0.01, 0.001, and 0.0001, respectively.

## 3. Results

### 3.1. Acute inflammatory response in the lung was induced by PM

The stimulation of the 4 PM types substantially increased the number of macrophages and neutrophils in BALF (Fig. 1). A significant increase in macrophages was observed 24 h after exposure to  $\geq 200 \mu\text{g}$  TiO<sub>2</sub>, 200  $\mu\text{g}$  ASD, and  $\geq 50 \mu\text{g}$  PM2.5 (Fig. 1A). Similarly, the neutrophil count increased in a concentration-dependent manner following the induction of an acute inflammatory response by PM. The significant infiltration of neutrophils ( $\geq 10^5$  cells/BALF) was observed when the exposure doses of TiO<sub>2</sub> were  $\geq 50 \mu\text{g}$  and those of DEP, ASD and PM2.5 were  $\geq 200 \mu\text{g}$  (Fig. 1B).

TNF- $\alpha$  expression in the BAL supernatant exhibited a concentration-dependent fold increase; 500  $\mu\text{g}$  TiO<sub>2</sub>, DEP, ASD and PM2.5 exposure resulted in 2.9-, 5.2-, 72.7- and 51.1-fold increases, respectively (Fig. 1C).

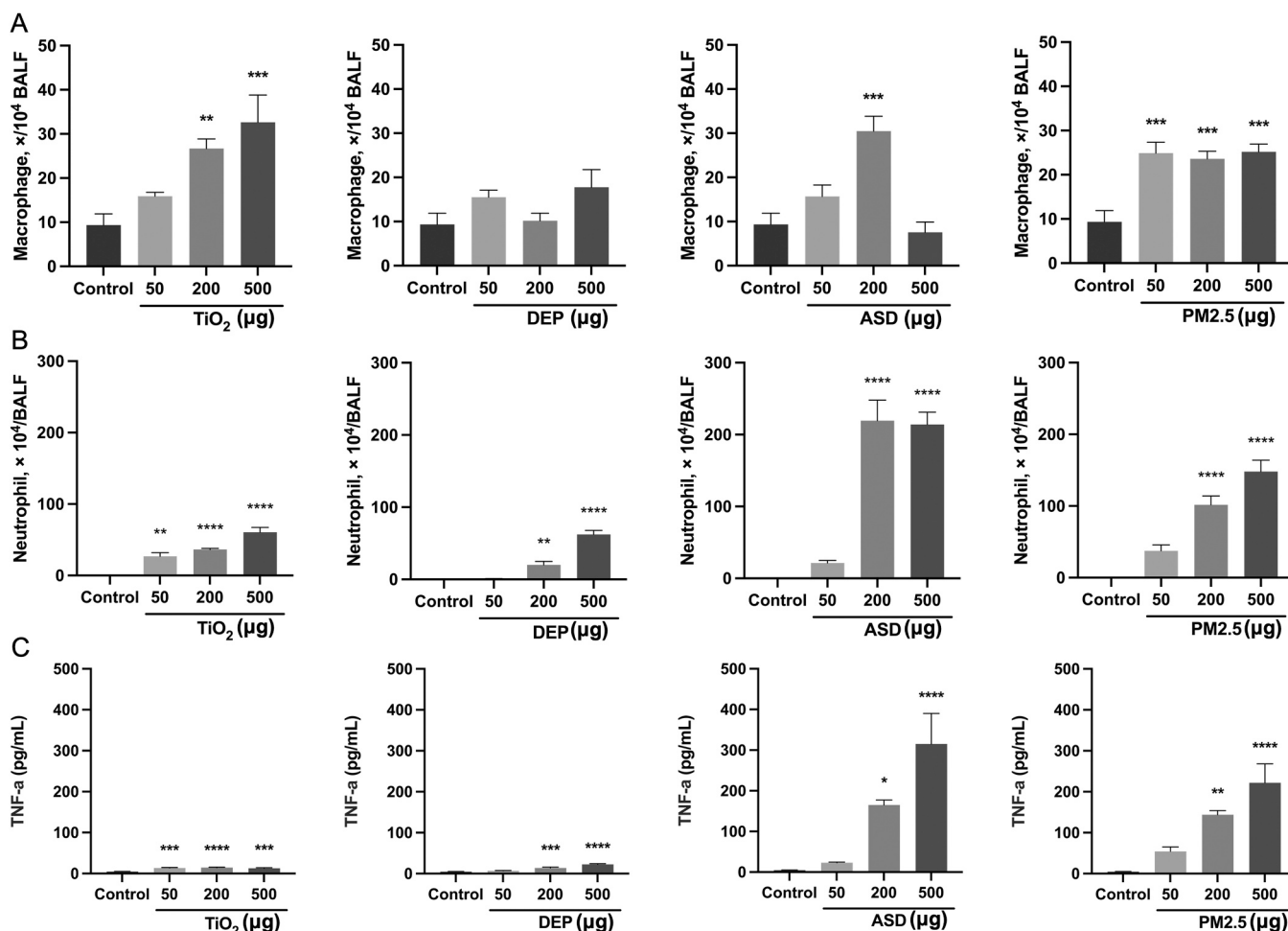


Fig. 1. Acute inflammatory response in the lung was induced by PM. *In vivo* experiments for the number of (A) macrophages, and (B) neutrophils in BALF induced by 50, 200, and 500  $\mu\text{g}/\text{mouse}$  of TiO<sub>2</sub>, DEP, ASD, and PM2.5. (C) *In vivo* experiments for determining TNF- $\alpha$  levels in BAL supernatants following administration of varying doses of four kinds of PM. Statistical significance is indicated as follows: \* $P < 0.05$ , \*\* $P < 0.01$ , \*\*\* $P < 0.001$  and \*\*\*\* $P < 0.0001$ , compared to the corresponding control group. TiO<sub>2</sub>: titanium dioxide, DEP: diesel exhaust particle, ASD: Asian sand dust, PM2.5: particulate matter with an aerodynamic diameter  $\leq 2.5 \mu\text{m}$ .

### 3.2. PM increased C5 protein levels in the lungs

To investigate the PM-induced influx of C5 into the lungs and its serum production, C5 content was detected in BAL supernatants and serum.

The four types of PM stimulation increased C5 levels in the BAL supernatants. In particular, exposure to 500  $\mu\text{g}$  ASD resulted in a 156-fold increase compared to the control. A significant influx of C5 was observed following exposure to  $\geq 200$   $\mu\text{g}$   $\text{TiO}_2$ , ASD, and  $\text{PM}_{2.5}$  and 500  $\mu\text{g}$  DEP (Fig. 2A). In contrast, serum C5 content showed no significant differences after exposure to the four particles (Fig. 2B).

### 3.3. PM increased the deposition of the terminal C5b-9 complement complex in lung tissue

C5b-9 IHC-specific staining of PM-challenged lung tissues (Fig. 3B-D) was compared with that of control lung tissues (Fig. 3A). The deposition of C5b-9 was slightly located in the bronchial epithelial cells in control mice (Fig. 3A). In contrast, it was located in the bronchial and alveolar epithelial cells, as well as some immune cells in  $\geq 200$   $\mu\text{g}$  ASD-, and 500  $\mu\text{g}$   $\text{PM}_{2.5}$ -, and DEP-challenged mice (Fig. 3C, D).

The semi-quantitative analysis of IHC staining demonstrated an upregulation of C5b-9 expression in the lung tissues after challenging with  $\geq 200$   $\mu\text{g}$  ASD (\* $P < 0.05$  and \*\*\* $P < 0.001$ ) and 500  $\mu\text{g}$  DEP (\*\* $P < 0.001$ ) and  $\text{PM}_{2.5}$  (\* $P < 0.05$ ) (Fig. 3E). The representative image scope analysis figures of C5b-9 are shown in Figure S1.

### 3.4. C5aR1 levels increased in lung tissues challenged with PM

C5aR1 IHC-specific staining in PM-challenged lung tissues (Fig. 4B-D) showed increased expression in 200  $\mu\text{g}$  and 500  $\mu\text{g}$  PM-treated mice compared to control lung tissues (Fig. 4A). C5aR1 expression was limited to a small number of immune cells in control lung tissues, whereas it was observed in various types of immune cells in PM-challenged mice.

The semi-quantitative analysis of IHC staining demonstrated statistically significant upregulation of C5aR1 expression in lung tissues

challenged with 500  $\mu\text{g}$  DEP (\*\* $P < 0.001$ ), and  $\geq 200$   $\mu\text{g}$   $\text{TiO}_2$  (\*\* $P < 0.001$  and \*\*\* $P < 0.0001$ ), ASD (\*\*\* $P < 0.0001$ ), and  $\text{PM}_{2.5}$  (\*\* $P < 0.001$  and \*\*\* $P < 0.0001$ ) (Fig. 4E). The representative image scope analysis figures for C5aR1 are shown in Figure S2.

### 3.5. C5aR1 was expressed in some lung macrophages, neutrophils, and dendritic cells following PM administration

To determine the PM-mediated C5aR1 expression levels in the lungs, we first evaluated neutrophils, which express this protein in high numbers (Karsten et al., 2015). To investigate the association between neutrophils and C5aR1-expressing cells, mouse lung tissues of the control and PM-challenged groups were stained with antibodies against the neutrophil markers Ly6G and C5aR1 (Fig. 5). Microscopy confirmed that a large number of Ly6G-positive neutrophils infiltrated the lungs following PM challenge, most of which expressed C5aR1. However, these cells were seldom detected in the control group.

Additional examination of F4/80 and C5aR1 expression in the identical lung tissue sections identified some of the C5aR1-expressing cells as F4/80-positive macrophages (Fig. 6).

Finally, we examined C5aR1 expression in lung dendritic cells, which also express C5aR1. Several dendritic cells (F4/80-negative and CD11c-positive cells) were C5aR1 positive after PM challenge (Fig. 7).

### 3.6. Localization of particles in lung tissues and their association with C5aR1-positive neutrophils in the ASD exposure group: Raman spectroscopy analysis

The 200  $\mu\text{g}$  ASD exposure group samples were used as a representative PM to detect the presence of particles in the vicinity of C5aR1-positive neutrophils. Dark-field and confocal Raman microscopy were used to determine the localization of particles in the lung tissue sections. The Raman signals of anatase-type  $\text{TiO}_2$  (Fig. 8A, D) and a phosphate mineral-wavellite ( $\text{Al}_3(\text{PO}_4)_2(\text{OH},\text{F})_3 \cdot 5 \text{H}_2\text{O}$ ) (Fig. 8A); a mixture of anatase, silica, and carbon (Fig. 8B); quartz ( $\text{SiO}_2$ ) (Fig. 8C); mica series minerals (Biotite  $\text{K}(\text{Mg},\text{Fe})_3\text{AlSi}_3\text{O}_{10}(\text{OH},\text{F})_2$ ; muscovite  $\text{KAl}_2[(\text{OH})_2/\text{AlSi}_3\text{O}_{10}]$ ) (Fig. 8C); and carbon (Fig. 8C), were detected in the vicinity

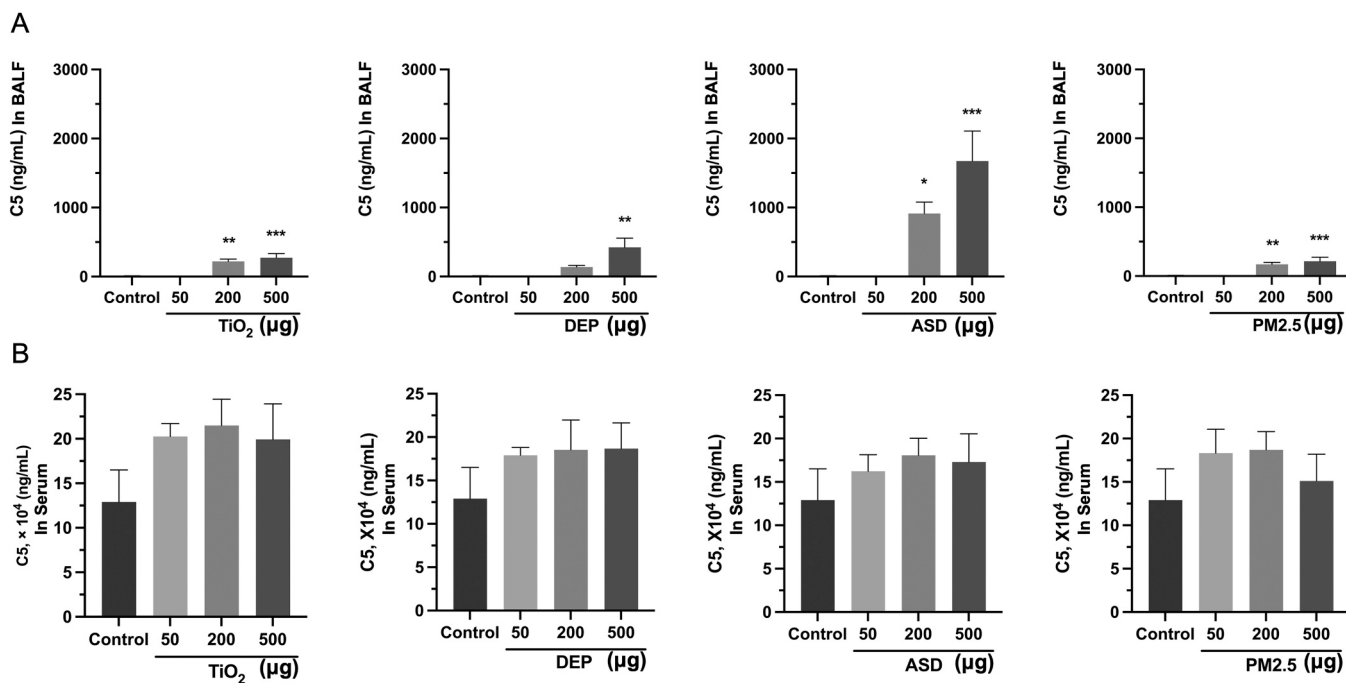
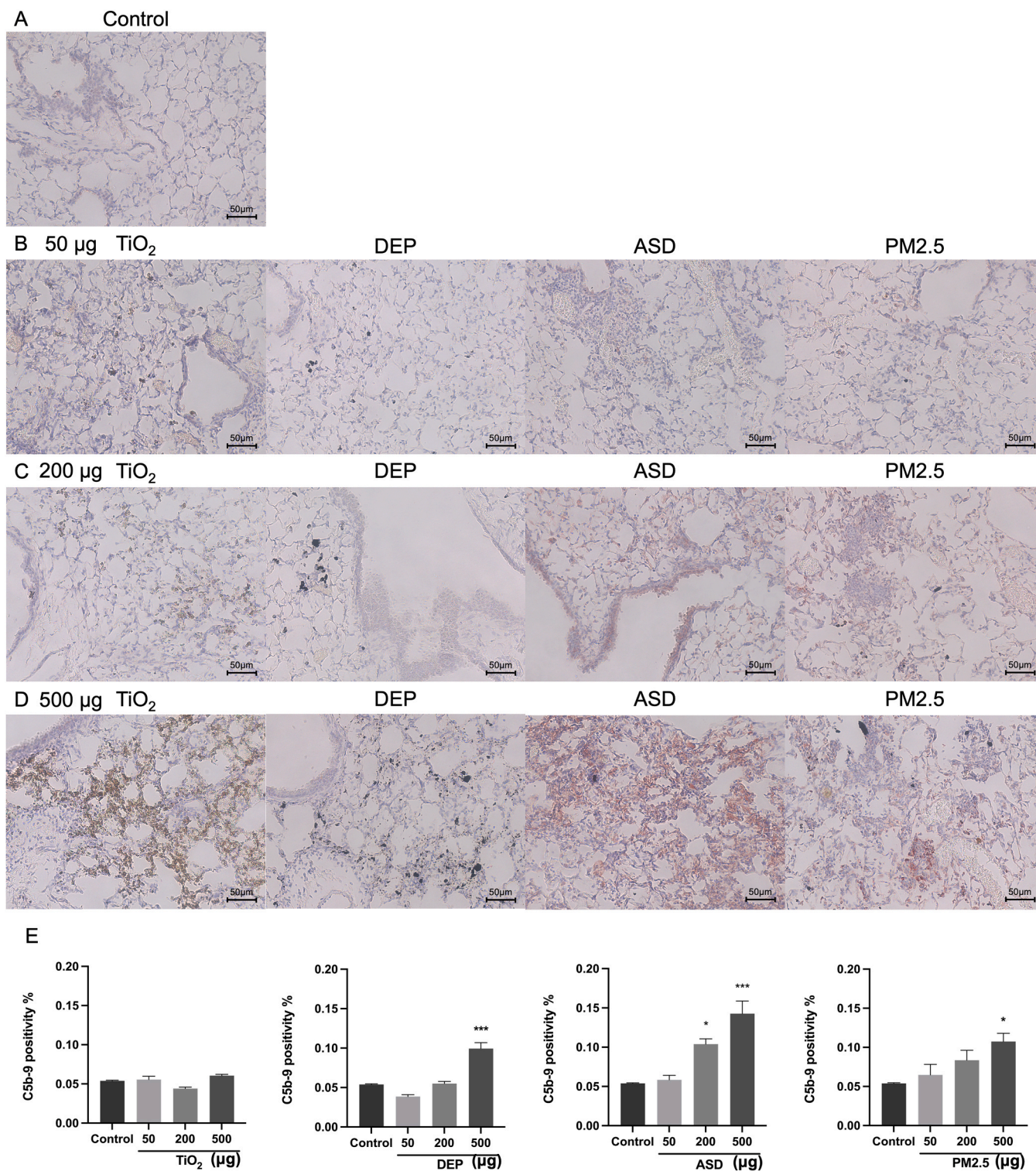


Fig. 2. C5 levels modulated by PM exposure. *In vivo* experiments for determining C5 levels in (A) BAL supernatants and (B) serum following administration of 50, 200, and 500  $\mu\text{g}/\text{mouse}$  of  $\text{TiO}_2$ , DEP, ASD, and  $\text{PM}_{2.5}$  particles. \* $P < 0.05$ , \*\* $P < 0.01$ , \*\*\* $P < 0.001$  and \*\*\*\* $P < 0.0001$ , compared to the corresponding control group.  $\text{TiO}_2$ : titanium dioxide, DEP: diesel exhaust particle, ASD: Asian sand dust,  $\text{PM}_{2.5}$ : particulate matter with an aerodynamic diameter  $\leq 2.5$   $\mu\text{m}$ .



**Fig. 3.** C5b-9 deposition induced by the administration of 50, 200, and 500 µg of TiO<sub>2</sub>, DEP, ASD, and PM2.5. Representative images of lung tissue sections from (A) control and at dosages of (B) 50 µg, (C) 200 µg, and (D) 500 µg of TiO<sub>2</sub>, DEP, ASD, and PM2.5 - challenged mice, as determined through immunohistochemical staining for C5b-9. (E) The positivity of C5b-9 in lung tissue cells was assessed with the Biosystem image scope software (regions = 60. The right lungs of three mice were selected in each group, and five sites were selected per lung lobe, resulting in a total of 3 × 4 × 5 = 60 sites). \*P < 0.05, \*\*P < 0.01, \*\*\*P < 0.001 and \*\*\*\*P < 0.0001, compared to the corresponding control group. Bar: 50 µm. TiO<sub>2</sub>: titanium dioxide, DEP: diesel exhaust particle, ASD: Asian sand dust, PM2.5: particulate matter with an aerodynamic diameter ≤ 2.5 µm.

of Ly6G<sup>+</sup> C5aR1<sup>+</sup> cells (neutrophils).

**3.7. Correlation analysis revealed elements of PM associated with acute inflammatory responses and complement system activation**

The volcano plots for TiO<sub>2</sub>, DEP, ASD, and PM2.5 were each

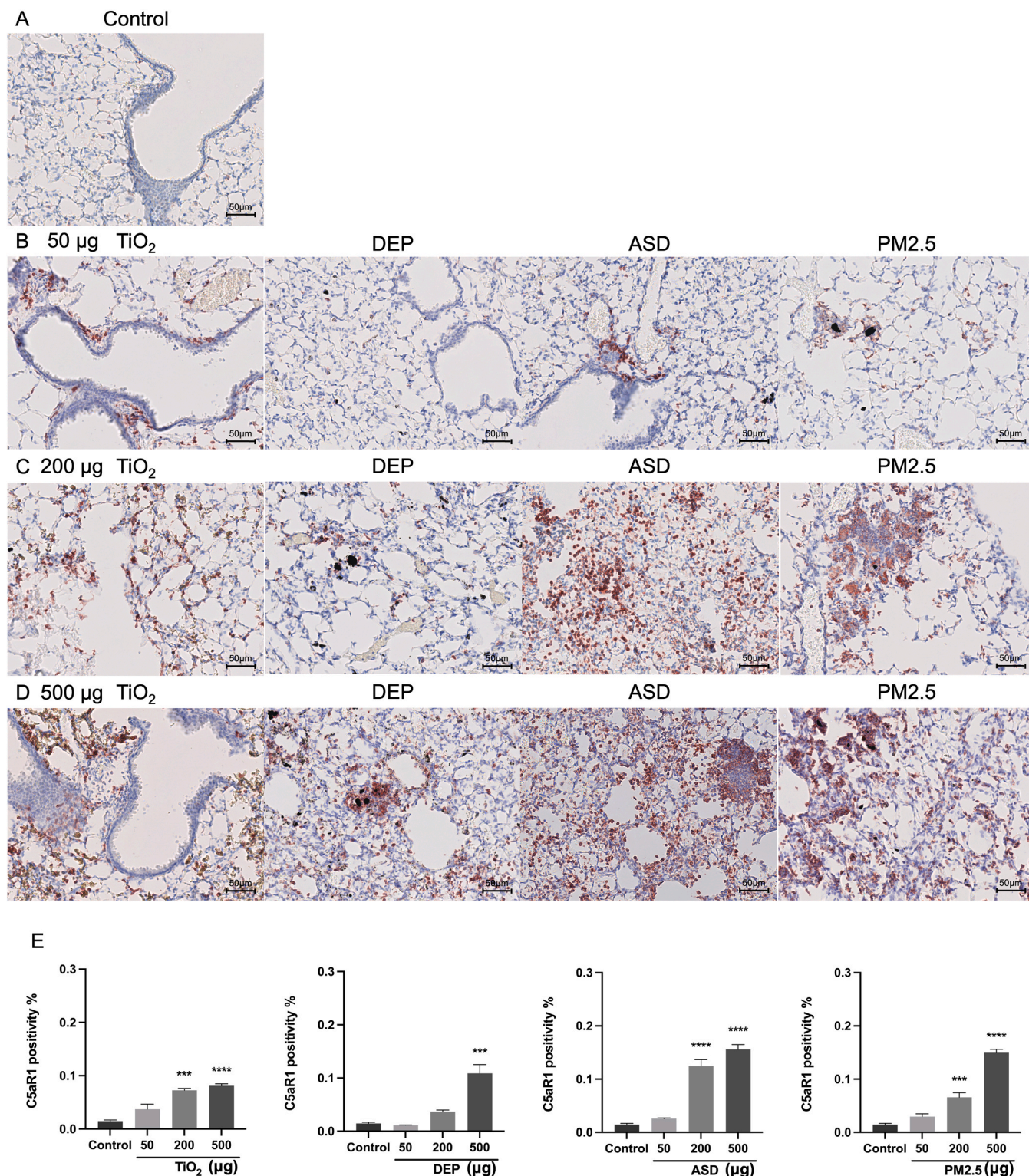


**Fig. 4.** C5aR1 expression induced by the administration of 50, 200, and 500 µg of TiO<sub>2</sub>, DEP, ASD, and PM2.5. Representative images of lung tissue sections from (A) control and (B) 50 µg, (C) 200 µg, and (D) 500 µg of TiO<sub>2</sub>, DEP, ASD, and PM2.5-challenged mice, as obtained through immunohistochemical staining for C5aR1. (E) The positivity of C5aR1 in lung tissue cells was assessed using the Biosystem image scope software (regions = 60 in each group). \*P < 0.05, \*\*P < 0.01, \*\*\*P < 0.001 and \*\*\*\*P < 0.0001, compared to the corresponding control group. Bar: 50 µm. TiO<sub>2</sub>: titanium dioxide, DEP: diesel exhaust particle, ASD: Asian sand dust, PM2.5: particulate matter with an aerodynamic diameter ≤ 2.5 µm.

compared with those for the control group (Figure S3). For ASD, all markers were higher on the horizontal and vertical axis, suggesting a more pronounced increase compared to the control group. As shown in the correlation heatmap, neutrophils, TNF-α, C5 in BALF, C5aR1

positivity, and C5b-9 positivity demonstrated positive correlations with various metal elements, particularly Si, Mg, Al, and K. Certain organic compounds (such as fluoranthene and pyrene) exhibited a negative correlation with inflammatory and complement system markers. Fig. 9

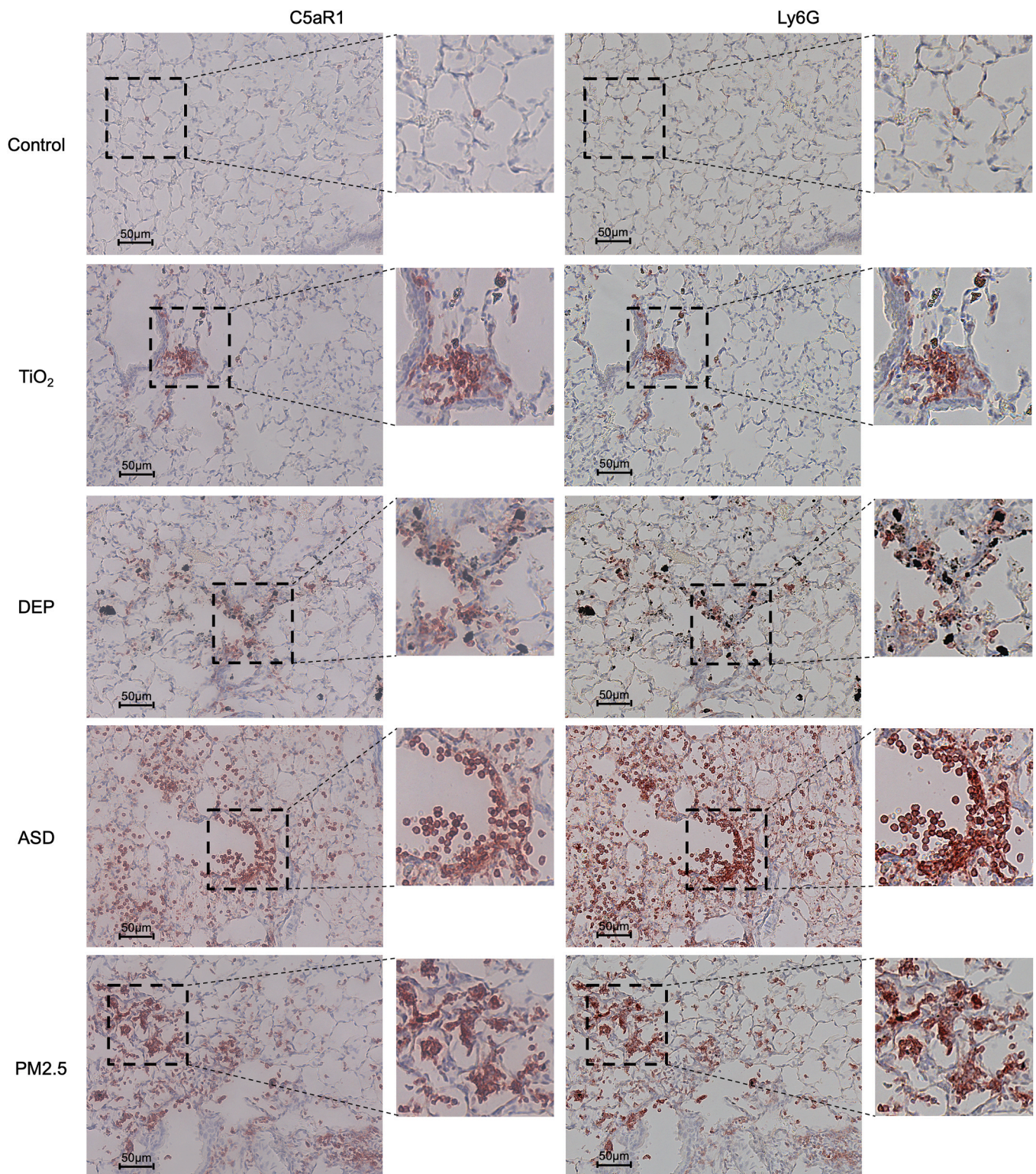


**Fig. 5.** C5aR1 expression in Ly6G positive cells (neutrophils) following the administration of 200 µg of TiO<sub>2</sub>, DEP, ASD, and PM2.5. Representative images of neutrophils of the lung tissue sections from control, TiO<sub>2</sub>, DEP, ASD, and PM2.5 groups. Bar: 50 µm. TiO<sub>2</sub>: titanium dioxide, DEP: diesel exhaust particle, ASD: Asian sand dust, PM2.5: particulate matter with an aerodynamic diameter ≤ 2.5 µm.

#### 4. Discussion

This study demonstrated that four types of PM—TiO<sub>2</sub>, DEP, ASD, and PM2.5—induced acute inflammatory responses and activated C5 and its related components in the lungs. Of these PM types, ASD caused the most significant C5b-9 deposition, upregulated C5aR1 expression in

neutrophils, and induced severe acute inflammatory responses in the lungs. Consequently, ASD exhibited the most potent ability to induce acute inflammatory responses and activate complement component C5. Additionally, its related compounds (i.e., TiO<sub>2</sub>, Wavellite, quartz, mica series minerals, and carbon) were detected in the vicinity of the aggregation of neutrophils. Thus, high Si, K, Mg, and Al contents may

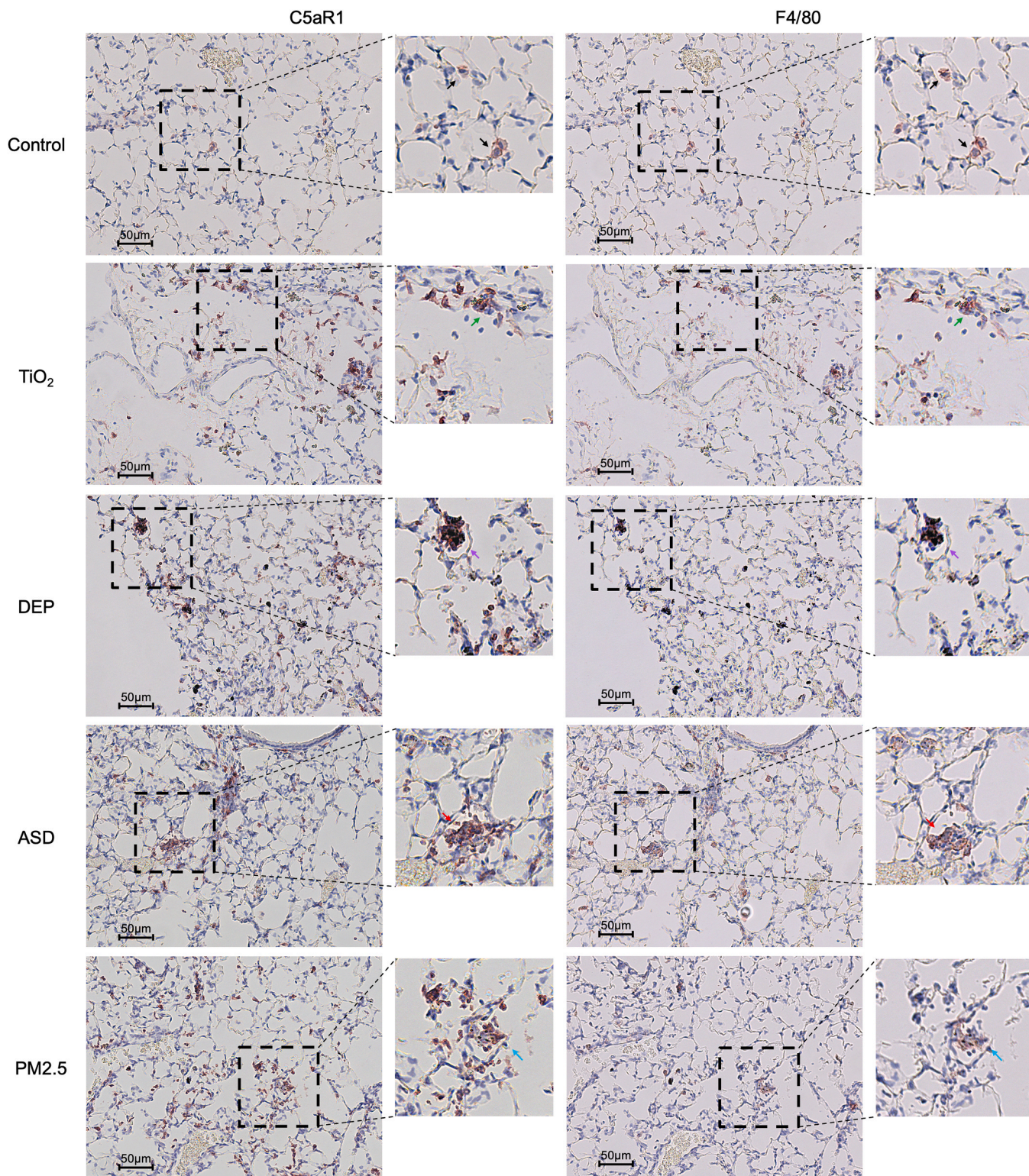


**Fig. 6.** C5aR1 expression in F4/80 positive cells (macrophages) following the administration of 200  $\mu\text{g}$  of  $\text{TiO}_2$ , DEP, ASD, and  $\text{PM}_{2.5}$ . Representative images of macrophages of the lung tissue sections from control (black arrow) and  $\text{TiO}_2$  (green arrow), DEP (purple arrow), ASD (red arrow), and  $\text{PM}_{2.5}$  (blue arrow) groups. Bar: 50  $\mu\text{m}$ .  $\text{TiO}_2$ : titanium dioxide, DEP: diesel exhaust particle, ASD: Asian sand dust,  $\text{PM}_{2.5}$ : particulate matter with an aerodynamic diameter  $\leq 2.5 \mu\text{m}$ .

contribute to acute inflammatory response and complement system activation.

The influx of polymorphonuclear neutrophils, a characteristic of acute inflammatory response (Castanheira and Kubes, 2019), along with  $\text{TNF-}\alpha$ , a critical mediator of inflammation, plays a key role in the mediation of particle-induced lung inflammation (Lai et al., 2019).

During inflammation,  $\text{TNF-}\alpha$  not only directly promotes the activation and recruitment of leukocytes but may also enhance the leukocyte response through feedback mechanisms (Norman et al., 2005). Therefore, both are often used as indicators of inflammatory response and are widely applied to evaluate acute inflammation models.

Macrophages may be recruited to particle deposition sites through a

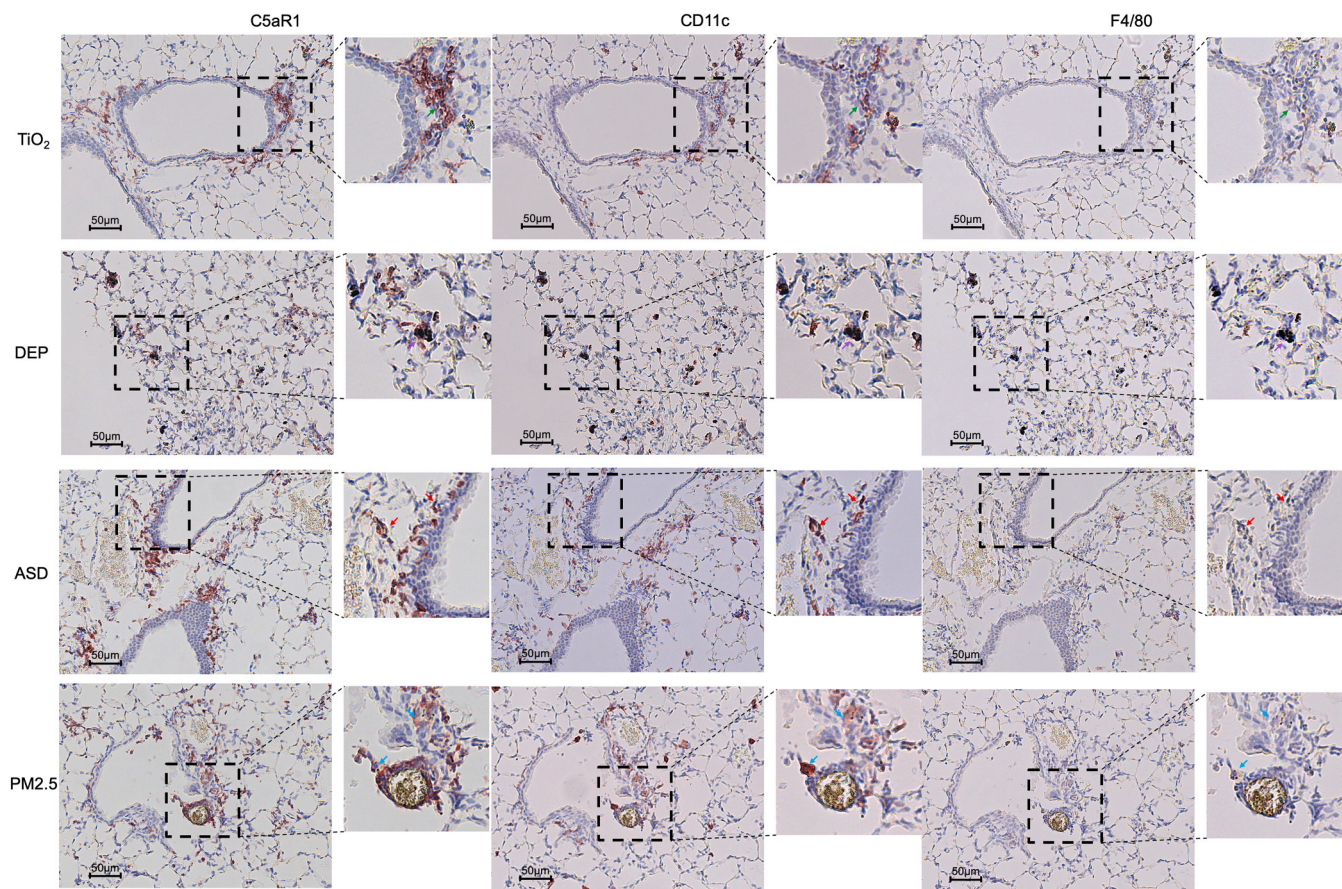


**Fig. 7.** C5aR1 expression in F4/80-negative and CD11c-positive cells (dendritic cells) following the administration of 200 µg of TiO<sub>2</sub>, DEP, ASD, and PM2.5. Representative images of dendritic cells of the lung tissue sections from control (black arrow) and TiO<sub>2</sub> (green arrow), DEP (purple arrow), ASD (red arrow), and PM2.5 (blue arrow) groups. Bar: 50 µm TiO<sub>2</sub>: titanium dioxide, DEP: diesel exhaust particle, ASD: Asian sand dust, PM2.5: particulate matter with an aerodynamic diameter ≤ 2.5 µm.

complement activation mechanism (Moghimi and Simberg, 2017) and are integral to the clearance of inhaled particles from the lungs and regulation of the inflammatory process. The intense accumulation of macrophages, predominant infiltration of neutrophils, and a P-value of < 0.05 for TNF-α concentration in this study indicate that exposure to ≥ 200 µg of TiO<sub>2</sub>, DEP, ASD, and PM2.5 particles induces an acute inflammatory response. However, the degree of acute inflammatory response varies significantly between different particles at the same dose. ASD particles are more effective in inducing macrophage accumulation and neutrophil infiltration than the other particles. Although exposure to TiO<sub>2</sub> and DEP significantly increased TNF-α levels (P < 0.05), the increases were relatively modest, with 500 µg TiO<sub>2</sub> and DEP leading to 2.9-fold and 5.2-fold increases, respectively. Exposure to 500 µg ASD and PM2.5 resulted in markedly larger increases, exceeding 72.7- and 51.1-fold, respectively. This demonstrates a substantially stronger inflammatory response than that elicited by TiO<sub>2</sub> and DEP. This may indicate differences in PM-stimulated inflammatory pathways, owing to significant differences in the chemical and physical characteristics of the particles.

We further analyzed C5, which generates the anaphylatoxins C5a and C5b after cleavage. C5a uniquely regulates lung inflammation and injury (e.g., chemotaxis, oxidative burst, and phagocytosis) by activating myeloid cells in the lungs (Sadik et al., 2018) (e.g., neutrophils, macrophages, and dendritic cells). TiO<sub>2</sub>, DEP, ASD, and PM2.5 activated the complement system and increased C5 concentration in the lungs; ASD caused the strongest elevation in C5 levels (Fig. 2A). This suggests that ASD has the potential to induce neutrophilic inflammation more intensely than other particles. Contrastingly, serum C5 levels showed no

significant differences compared to the control group after exposure to TiO<sub>2</sub>, DEP, ASD, and PM2.5 (Fig. 2B). This suggests that the systemic response may be less pronounced, or that the inflammatory effects were primarily localized to the lung tissues without substantially affecting the bloodstream.

In addition to C5, we evaluated the expression of the terminal C5b-9 complement complex in the lungs of TiO<sub>2</sub>, DEP-, ASD-, and PM2.5-challenged mice. ASD samples exhibited C5b-9 aggregation at both medium and high doses during semi-quantitative analysis, which may trigger excessive activation of the complement system (Fattahi et al., 2020) and excessive accumulation of the complement terminal component C5b-9 (Guo et al., 2022; Keshari et al., 2017). MAC may induce cell damage and death (Woodruff et al., 2011) and exert several non-cytolytic effects that actively promote inflammation. It induces the expression of adhesion molecules, facilitates the release of chemokines (Dobrina et al., 2002), and triggers intracellular calcium fluxes, as well as activation of the NLRP3 inflammasome (Malsy et al., 2020). These actions contribute to cell and organ dysfunction (Fattahi et al., 2020), particularly by targeting bronchial epithelial cells, alveolar epithelial cells, and various immune cells, thereby amplifying the inflammatory response.

C5aR1 is expressed by immune cells such as neutrophils, macrophages, and dendritic cells (Karsten et al., 2015; Ender et al., 2017). Most of the C5a functional effects are achieved by combining it with C5aR1 (Lee et al., 2008). This necessitated the investigation of the cell types and changes in C5aR1 expression after the four types of PM challenges. TiO<sub>2</sub>, DEP, ASD, and PM2.5 all elicited an increase in and aggregation of cells expressing C5aR1 (Fig. 4B), with ASD exposure

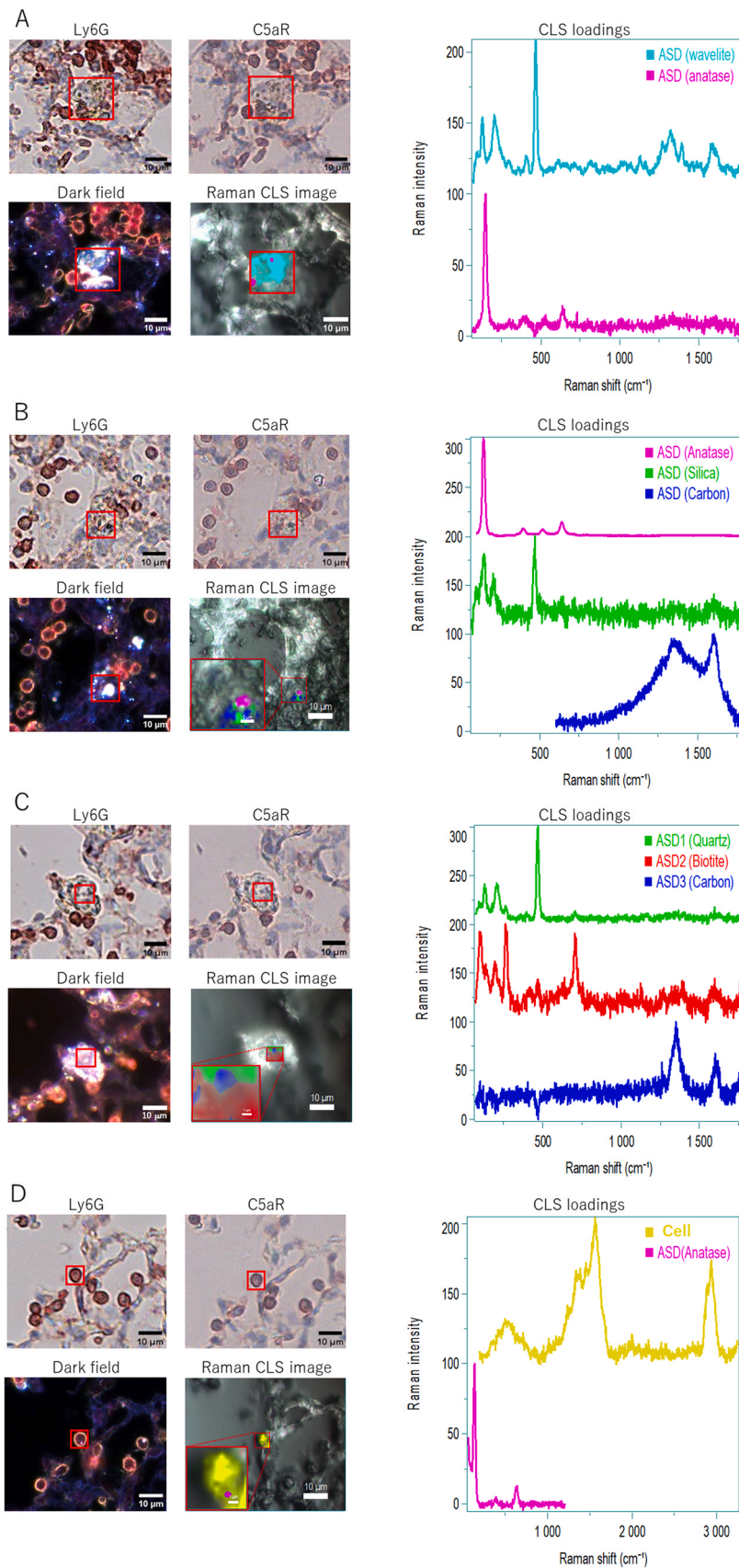


**Fig. 8.** Darkfield and confocal Raman image analysis of particles in the vicinity of C5aR1<sup>+</sup> neutrophils after 200 µg ASD challenge. (A) Anatase and wavelite signal. (B) Anatase, silica and carbon signal. (C) Quartz, biotite, and carbon signal. (D) Raman signals of anatase were detected in Ly6G<sup>+</sup>C5aR1<sup>+</sup> cells. Database of specific Raman bands, Raman-Forensic-HORIBA. ASD: Asian sand dust.

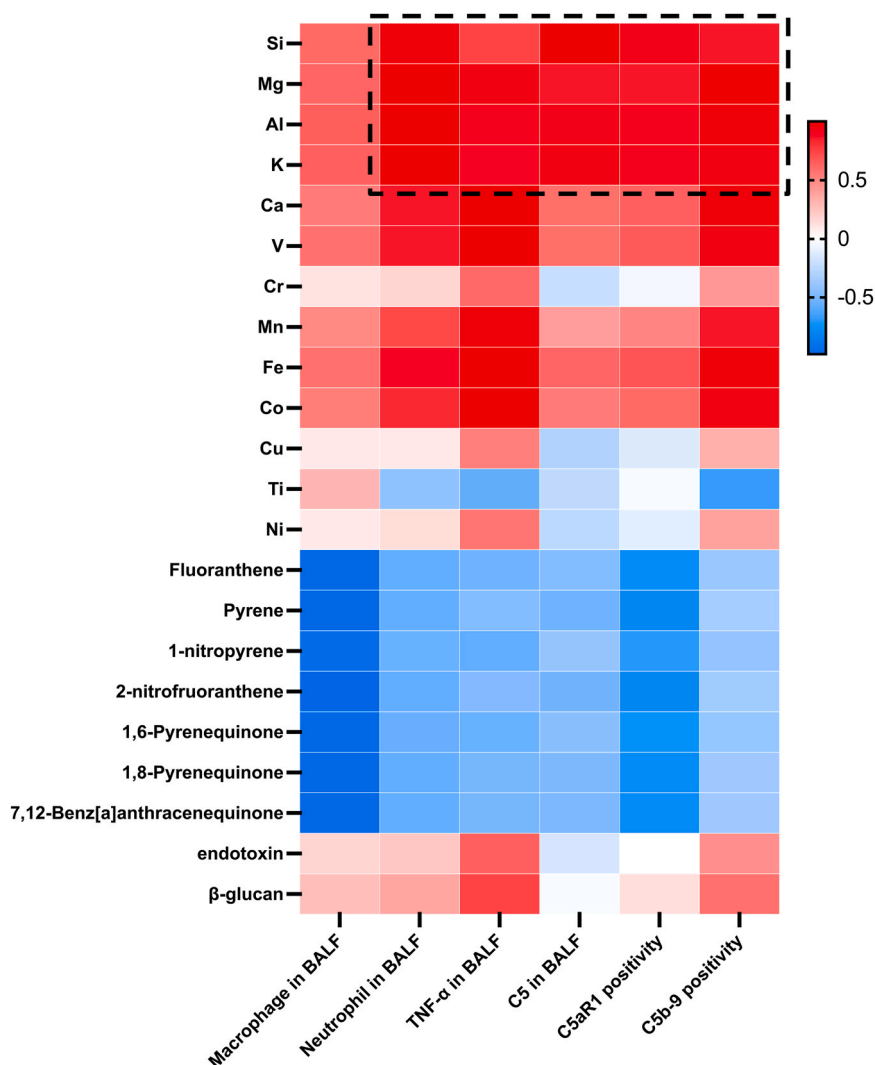


**Fig. 9.** Heat map of the correlation among macrophage number in BALF, neutrophils number in BALF, TNF- $\alpha$  concentration in BALF, C5 concentration in BALF, C5aR1 positivity %, and C5b-9 positivity % and TiO<sub>2</sub>, DEP, ASD, and PM2.5 components. The results within the dashed rectangular box in the figure are highlighted for emphasis due to high positive correlation between components and biological responses. TiO<sub>2</sub>: titanium dioxide, DEP: diesel exhaust particle, ASD: Asian sand dust, PM2.5: particulate matter with an aerodynamic diameter  $\leq 2.5 \mu\text{m}$ .

resulting in the highest number of C5aR1-expressing cells (Fig. 4E). Moreover, the morphological analysis of C5aR1-expressing cells revealed that they belong to different immune cell types (Figs. 5, 6, 7).

The Ly6G marker can be used to distinguish neutrophils (Christofides et al., 2021), whereas the CD11c and F4/80 markers (Misharin et al., 2013; Zaynagetdinov et al., 2013) can effectively distinguish dendritic cells from other myeloid cells in the lungs of healthy mice. Consequently, dendritic cells were identified by staining with CD11c and F4/80. The functional role of C5aR1 is closely associated with the cell types upon which it is expressed (Lee et al., 2008). In this study, infiltration of neutrophils in the lungs was prevalent after PM exposure. Additionally, these cells aggregated in the vicinity of the ASD particles. This aggregation may be driven by several mechanisms: PM exposure triggers nearby cells, particularly bronchial epithelial, alveolar epithelial, and immune cells, leading to the release of cytokines and chemokines that promote the recruitment of neutrophils. It also induces oxidative stress, consequently increasing ROS production, which further enhances the expression of inflammation-related cytokines and strengthens neutrophil aggregation (Valderrama et al., 2022). Additionally, PM stimulates the release of NETs by neutrophils through their DNA and protein components, which promote platelet aggregation and exacerbate local inflammation (Elaskalani et al., 2018). Neutrophils,

which are the most prevalent C5aR1-expressing cells, may be the most important cells, as they respond to PM-induced acute inflammation through C5a-C5aR1 signaling. However, some macrophages and dendritic cells also expressed C5aR1 and may be important in the regulation of acute inflammatory responses via the same signaling pathway.

In our previous study (Chowdhury et al., 2019), crude PM2.5 exhibited more profound pro-inflammatory effects than its aqueous and organic extracts, demonstrating that PM plays an indispensable role in the pro-inflammatory process. Therefore, the ASD 200  $\mu\text{g}/\text{mouse}$  exposure group, which exhibited the most significant neutrophil infiltration, was selected to determine whether ASD particles were present in the vicinity of neutrophil aggregates. ASD particles are mainly composed of Si, K, Mg, and Al. Other potentially toxic chemicals may be introduced during long-distance transportation, including soil-derived microorganisms and industrial pollution (Fussell and Kelly, 2021). We identified representative inorganic compounds and carbon in ASD particles in the vicinity of neutrophil aggregates (Fig. 8A-C). In addition, we theorized that the Raman signal of anatase TiO<sub>2</sub> detected in Ly6G<sup>+</sup>C5aR1<sup>+</sup> cells originated from ASD particles phagocytosed by neutrophils (Fig. 8D). Silicon oxides (Ding and Sun, 2020; Park et al., 2020) and compounds of the metal elements Mg (Feyerabend et al., 2015) and Al (Güven et al., 2013) can activate the complement system.

The higher concentrations of these elements in ASD than in other PM may partly explain why ASD can cause severe acute inflammatory reactions and complement system activation. Quartz (containing SiO<sub>2</sub>), wavellite (containing Al), and mica series minerals (containing Mg, Al, and Si) found in the vicinity of aggregated neutrophils may have acted as contributing components that triggered acute inflammatory responses and activated the complement system.

To elucidate the molecular changes induced by PM exposure, volcano plots were utilized to illustrate the differential expression of inflammatory and complement system markers. Neutrophils were most prominently upregulated in response to PM exposure, especially in the ASD group. This highlights their central role in the immune response. TNF- $\alpha$  levels were significantly increased across all conditions, reflecting the general involvement of this cytokine in inflammation. C5aR1 and C5 concentrations in BALF were upregulated in all PM treatments, with the most significant effect observed in the ASD group, indicating complement system activation as a key mechanism in the immune effects of PM exposure.

Consistent with the Raman spectroscopy results, the color changes observed between inflammatory (Macrophages, Neutrophils, and TNF- $\alpha$ ) and complement system (C5 in BALF, C5aR1 positivity, and C5b-9 positivity) markers in the correlation heatmap suggest that minerals such as Si, Mg, Al, K may contribute to acute inflammatory responses and complement system activation. PAH components exhibited a negative correlation with these markers. This may be because the acute inflammatory response triggered by PAHs-rich DEP is less pronounced than that induced by ASD and PM<sub>2.5</sub>, which contain lower levels of organic chemical compounds and higher concentrations of metal elements. This could also suggest that the effect of minerals on the acute inflammatory response and complement system activation is stronger than that of organic chemical compounds. Similarly, endotoxin and  $\beta$ -glucan show consistent patterns with inflammatory indicators and C5b-9 positivity, implying a possible contribution to acute inflammatory responses and C5b-9 deposition. Compared to the elements, endotoxin and  $\beta$ -glucan exhibit distinct grouping differences in complement-related indicators (C5aR1 positivity and C5 concentration in BALF), which may suggest a more specific association with C5b-9 deposition. Nonetheless, further investigation is required to confirm these observations. In particular, future studies are required to explore the dose-dependent effects of individual minerals, endotoxin, and  $\beta$ -glucan on inflammatory markers and complement activation, as well as identify the molecular pathways involved in the activation of the complement system during PM exposure. This study has certain limitations. The experimental approach relied on an in vivo animal exposure model, which did not allow for in-depth investigation of cell-type-specific responses to complement system activation induced by PM exposure. Future studies could isolate specific cell types (e.g., neutrophils, macrophages, and dendritic cells) for in vitro experiments to further validate the findings of this research.

## 5. Conclusion

To our knowledge, this study is the first to demonstrate that 4 PM types with different compositions can induce acute inflammatory responses and complement system activation upon respiratory exposure. Of the tested PM types, ASD exposure caused the most severe innate immune dysfunction and early proinflammatory responses. These findings emphasize the importance of characterizing PM composition and its specific impacts on health. This study highlights the differential activation of key complement components (C5, C5aR1, and C5b-9) by various PM types, consequently providing insights into the mechanisms underlying acute inflammation. Raman spectroscopy analysis revealed the minerals adjacent to infiltrating neutrophils, with C5aR1 identified in ASD-exposed lungs. However, future research should identify the specific PM components responsible for these effects and their roles in lung-related conditions such as asthma and tissue damage, considering the

complexity and variability of PM sources.

## CRediT authorship contribution statement

**Zhang Kerui:** Writing – original draft, Visualization, Investigation, Formal analysis, Data curation, Conceptualization. **Ichinose Takamichi:** Writing – review & editing, Supervision, Investigation. **Takano Hirohisa:** Writing – review & editing, Supervision, Funding acquisition, Conceptualization. **Miyasaka Natsuko:** Writing – review & editing, Investigation. **Qiu Binyang:** Writing – review & editing, Investigation. **Honda Akiko:** Writing – review & editing, Supervision, Project administration, Investigation. **Sagawa Tomoya:** Writing – review & editing, Investigation. **Kameda Takayuki:** Writing – review & editing, Supervision, Investigation. **Sadakane Kaori:** Writing – review & editing, Supervision, Investigation. **Ishikawa Raga:** Writing – review & editing, Supervision, Investigation. **Okuda Tomoaki:** Writing – review & editing, Supervision, Resources, Investigation.

## Consent for publication

Not applicable.

## Ethics approval and consent to participate

The study adhered to the Animal Research Reporting of in Vivo Experiments (ARRIVE) and the United States National Institutes of Health guidelines on the use of experimental animals. In addition, the animal protocols were reviewed and approved by the Animal Care and Use Committee of the Oita University of Nursing and Health Sciences, Oita, Japan. (approval number: 20–88).

## Funding

This work was supported by the Core Research for Evolutional Science and Technology (CREST) program of the Japan Science and Technology Agency (JST), Japan [grant number JPMJCR19H3].

## Declaration of Competing Interest

The authors declare that they have no known competing financial interests or personal relationships that could have appeared to influence the work reported in this paper.

## Acknowledgments

We thank Yinpeng Li and Pasunun Rattanaroongrot for their technical assistance.

## Appendix A. Supporting information

Supplementary data associated with this article can be found in the online version at [doi:10.1016/j.ecoenv.2025.118259](https://doi.org/10.1016/j.ecoenv.2025.118259).

## Data availability

Data will be made available on request.

## References

- Akaji, S., Sagawa, T., Honda, A., et al., 2022. Post-staining Raman analysis of histological sections following decolorization. *Analyst* 147 (20), 4473–4479.
- Antoniou, K., Ender, F., Vollbrandt, T., et al., 2020. Allergen-induced C5a/C5aR1 axis activation in pulmonary CD11b+ cDCs promotes pulmonary tolerance through downregulation of CD40. *Cells* 9 (2), 300.
- Atkinson, R., Cohen, A., Mehta, S., Anderson, H., 2012. Systematic review and meta-analysis of epidemiological time-series studies on outdoor air pollution and health in Asia. *Air Qual., Atmosphere Health* 5, 383–391.

- Baisch, B.L., Corson, N.M., Wade-Mercer, P., et al., 2014. Equivalent titanium dioxide nanoparticle deposition by intratracheal instillation and whole body inhalation: the effect of dose rate on acute respiratory tract inflammation. *Part. Fibre Toxicol.* 11 (1), 1–16.
- Benmerzoug, S., Rose, S., Bounab, B., et al., 2018. STING-dependent sensing of self-DNA drives silica-induced lung inflammation. *Nat. Commun.* 9 (1), 5226.
- Braakhuis, H.M., Gogens, I., Heringa, M.B., et al., 2021. Mechanism of action of TiO<sub>2</sub>: recommendations to reduce uncertainties related to carcinogenic potential. *Annu. Rev. Pharmacol. Toxicol.* 61 (1), 203–223.
- Castanheira, F.V., Kubers, P., 2019. Neutrophils and NETs in modulating acute and chronic inflammation. *Blood, J. Am. Soc. Hematol.* 133 (20), 2178–2185.
- Chen, J., Rodopoulou, S., de Hoogh, K., et al., 2021. Long-term exposure to fine particle elemental components and natural and cause-specific mortality—a pooled analysis of eight European cohorts within the ELAPSE project. *Environ. Health Perspect.* 129 (4), 047009.
- Choi, M.S., Jeon, H., Yoo, S.-M., Lee, M.-S., 2021. Activation of the complement system on human endothelial cells by urban particulate matter triggers inflammation-related protein production. *Int. J. Mol. Sci.* 22 (7), 3336.
- Chowdhury, P.H., Honda, A., Ito, S., et al., 2019. Effects of ambient PM<sub>2.5</sub> collected using cyclonic separator from Asian cities on human airway epithelial cells. *Aerosol Air Qual. Res.* 19 (8), 1808–1819.
- Christofides, A., Cao, C., Pal, R., Aksoylar, H.I., Boussiotis, V.A., 2021. Flow cytometric analysis for identification of the innate and adaptive immune cells of murine lung. *J. Vis. Exp.: JoVE* (177). <https://doi.org/10.3791/62985>.
- Ding, T., Sun, J., 2020. Formation of protein corona on nanoparticle affects different complement activation pathways mediated by C1q. *Pharm. Res.* 37 (1), 10.
- Dobrina, A., Pausa, M., Fischetti, F., et al., 2002. Cytolytically inactive terminal complement complex causes transendothelial migration of polymorphonuclear leukocytes in vitro and in vivo. *Blood, J. Am. Soc. Hematol.* 99 (1), 185–192.
- Dunkelberger, J.R., Song, W.-C., 2010. Complement and its role in innate and adaptive immune responses. *Cell Res.* 20 (1), 34–50.
- Ehrnthaller, C., Braumüller, S., Kellermann, S., Gebhard, F., Perl, M., Huber-Lang, M., 2021. Complement factor C5a inhibits apoptosis of neutrophils—a mechanism in polytrauma? *J. Clin. Med.* 10 (14), 3157.
- Elaskalani, O., Abdul Razak, N.B., Metharom, P., 2018. Neutrophil extracellular traps induce aggregation of washed human platelets independently of extracellular DNA and histones. *Cell Commun. Signal.* 16, 1–15.
- Ender, F., Wiese, A.V., Schmudde, I., et al., 2017. Differential regulation of C5a receptor 1 in innate immune cells during the allergic asthma effector phase. *PLoS One* 12 (2), e0172446.
- Falcon-Rodríguez, C.I., Osornio-Vargas, A.R., Sada-Ovalle, I., Segura-Medina, P., 2016. Aeroparticles, composition, and lung diseases. *Front. Immunol.* 7, 3.
- Fattahi, F., Zetoune, F.S., Ward, P.A., 2020. Complement as a major inducer of harmful events in infectious sepsis. *Shock (Augusta, Ga)* 54 (5), 595.
- Feyerabend, F., Wendel, H.-P., Mihailova, B., et al., 2015. Blood compatibility of magnesium and its alloys. *Acta Biomater.* 25, 384–394.
- Fujitani, Y., Hirano, S., Kobayashi, S., et al., 2009. Characterization of dilution conditions for diesel nanoparticle inhalation studies. *Inhal. Toxicol.* 21 (3), 200–209.
- Fussell, J.C., Kelly, F.J., 2021. Mechanisms underlying the health effects of desert sand dust. *Environ. Int.* 157, 106790.
- Ghobakhloo, S., Mostafaei, G.R., Khoshakhlagh, A.H., Moda, H.M., Gruszecka-Kosowska, A., 2024. Health risk assessment of heavy metals in exposed workers of municipal waste recycling facility in Iran. *Chemosphere* 346, 140627.
- Ghobakhloo, S., Khoshakhlagh, A.H., Mostafaei, G.R., Carlsen, L., 2025. Biomonitoring of metals in the blood and urine of waste recyclers from exposure to airborne fine particulate matter (PM<sub>2.5</sub>). *J. Environ. Health Sci. Eng.* 23 (1), 1–22.
- Guo, J., Liu, Q.-Z., Zhu, F.-J., et al., 2022. Acteoside attenuates acute lung injury following administration of cobra venom factor to mice. *Heliyon* 8 (11).
- Güven, E., Duus, K., Laursen, I., Højrup, P., Houen, G., 2013. Aluminum hydroxide adjuvant differentially activates the three complement pathways with major involvement of the alternative pathway. *PLoS One* 8 (9), e74445.
- He, M., Ichinose, T., Song, Y., et al., 2016. Desert dust induces TLR signaling to trigger Th2-dominant lung allergic inflammation via a MyD88-dependent signaling pathway. *Toxicol. Appl. Pharmacol.* 296, 61–72.
- He, M., Ichinose, T., Yoshida, S., et al., 2017. PM<sub>2.5</sub>-induced lung inflammation in mice: Differences of inflammatory response in macrophages and type II alveolar cells. *J. Appl. Toxicol.* 37 (10), 1203–1218.
- Honda, A., Okuda, T., Nagao, M., Miyasaka, N., Tanaka, M., Takano, H., 2021. PM<sub>2.5</sub> collected using cyclonic separation causes stronger biological responses than that collected using a conventional filtration method. *Environ. Res.* 198, 110490.
- Hovland, A., Jonasson, L., Garred, P., et al., 2015. The complement system and toll-like receptors as integrated players in the pathophysiology of atherosclerosis. *Atherosclerosis* 241 (2), 480–494.
- Hu, R., Chen, Z., Yan, J., et al., 2014. Complement C5a exacerbates acute lung injury induced through autophagy-mediated alveolar macrophage apoptosis. *Cell Death Dis.* 5 (7), e1330. e1330.
- Hu, X., Li, X., Hu, C., et al., 2017. Respiratory syncytial virus exacerbates OVA-mediated asthma in mice through C5a-C5aR regulating CD4<sup>+</sup> T cells immune responses. *Sci. Rep.* 7 (1), 15207.
- Husain, M., Wu, D., Saber, A.T., et al., 2015. Intratracheally instilled titanium dioxide nanoparticles translocate to heart and liver and activate complement cascade in the heart of C57BL/6 mice. *Nanotoxicology* 9 (8), 1013–1022.
- Jin, X., Ma, Q., Sun, Z., et al., 2019. Airborne fine particles induce hematological effects through regulating the crosstalk of the kallikrein-kinin, complement, and coagulation systems. *Environ. Sci. Technol.* 53 (5), 2840–2851.
- Kalbitz, M., Karbach, M., Braumueller, S., et al., 2016. Role of complement C5 in experimental blunt chest trauma-induced septic acute lung injury (ALI). *PLoS One* 11 (7), e0159417.
- Karsten, C.M., Laumonnier, Y., Eurich, B., et al., 2015. Monitoring and cell-specific deletion of C5aR1 using a novel floxed GFP-C5aR1 reporter knock-in mouse. *J. Immunol.* 194 (4), 1841–1855.
- Keshari, R.S., Silasi, R., Popescu, N.I., et al., 2017. Inhibition of complement C5 protects against organ failure and reduces mortality in a baboon model of Escherichia coli sepsis. *Proc. Natl. Acad. Sci.* 114 (31), E6390–E6399.
- Lai, W.-Y., Wang, J.-W., Huang, B.-T., Lin, E.P.-Y., Yang, P.-C., 2019. A novel TNF- $\alpha$ -targeting aptamer for TNF- $\alpha$ -mediated acute lung injury and acute liver failure. *Theranostics* 9 (6), 1741.
- Lee, H., Whitfield, P.L., Mackay, C.R., 2008. Receptors for complement C5a. The importance of C5aR and the enigmatic role of C5L2. *Immunol. Cell Biol.* 86 (2), 153–160.
- Lin, H., Chen, M., Gao, Y., Wang, Z., Jin, F., 2022. Tussilagonone protects acute lung injury from PM<sub>2.5</sub> via alleviating Hif-1 $\alpha$ /NF- $\kappa$ B-mediated inflammatory response. *Environ. Toxicol.* 37 (5), 1198–1210.
- Malsy, J., Alvarado, A.C., Lamontagne, J.O., Strittmatter, K., Marneros, A.G., 2020. Distinct effects of complement and of NLRP3- and non-NLRP3 inflammasomes for choroidal neovascularization. *Elife* 9, e60194.
- Misharin, A.V., Morales-Nebreda, L., Mutlu, G.M., Budinger, G.S., Perlman, H., 2013. Flow cytometric analysis of macrophages and dendritic cell subsets in the mouse lung. *Am. J. Respir. Cell Mol. Biol.* 49 (4), 503–510.
- Moghimi, S., Simberg, D., 2017. Complement activation turnover on surfaces of nanoparticles. *Nano Today* 15, 8–10.
- Morozaan, A., Joy, S., Fujii, U., et al., 2023. Superiority of systemic bleomycin to intradermal HOCl for the study of interstitial lung disease. *Sci. Rep.* 13 (1), 20577.
- Müller-Redetzky, H., Kellermann, U., Wienhold, S.-M., et al., 2020. Neutralizing complement C5a protects mice with pneumococcal pulmonary sepsis. *Anesthesiology* 132 (4), 795–807.
- Nakamura, R., Inoue, K.-i., Fujitani, Y., Kiyono, M., Hirano, S., Takano, H., 2012. Effects of nanoparticle-rich diesel exhaust particles on IL-17 production in vitro. *J. Immunotoxicol.* 9 (1), 72–76.
- Naota, M., Shiotsu, S., Shimada, A., et al., 2013. Pathological study of chronic pulmonary toxicity induced by intratracheally instilled Asian sand dust (kosa). *Toxicol. Pathol.* 41 (1), 48–62.
- Norman, M.U., Lister, K.J., Yang, Y.H., Issekutz, A., Hickey, M.J., 2005. TNF regulates leukocyte-endothelial cell interactions and microvascular dysfunction during immune complex-mediated inflammation. *Br. J. Pharmacol.* 144 (2), 265.
- Okuda, T., 2013. Measurement of the specific surface area and particle size distribution of atmospheric aerosol reference materials. *Atmos. Environ.* 75, 1–5.
- Okuda, T., Takada, H., Kumata, H., et al., 2013. Inorganic chemical characterization of aerosols in four Asian mega-cities. *Aerosol Air Qual. Res.* 13 (2), 436–449.
- Okuda, T., Schauer, J.J., Shafer, M.M., 2014. Improved methods for elemental analysis of atmospheric aerosols for evaluating human health impacts of aerosols in East Asia. *Atmos. Environ.* 97, 552–555.
- Park, J.H., Jackman, J.A., Ferhan, A.R., et al., 2020. Cloaking silica nanoparticles with functional protein coatings for reduced complement activation and cellular uptake. *ACS nano* 14 (9), 11950–11961.
- Reis, E.S., Mastellos, D.C., Hajishengallis, G., Lambris, J.D., 2019. New insights into the immune functions of complement. *Nat. Rev. Immunol.* 19 (8), 503–516.
- Rosa, M.J., Benedetti, C., Peli, M., et al., 2016. Association between personal exposure to ambient metals and respiratory disease in Italian adolescents: a cross-sectional study. *BMC Pulm. Med.* 16 (1), 1–9.
- Sadakane, K., Ichinose, T., Maki, T., Nishikawa, M., 2022. Co-exposure of peptidoglycan and heat-inactivated Asian sand dust exacerbates ovalbumin-induced allergic airway inflammation in mice. *Inhal. Toxicol.* 34 (9-10), 231–243.
- Sadik, C.D., Miyabe, Y., Sezin, T., Luster, A.D., 2018. The critical role of C5a as an initiator of neutrophil-mediated autoimmune inflammation of the joint and skin. *Elsevier* 21–29.
- Sagawa, T., Honda, A., Ishikawa, R., et al., 2021. Role of necroptosis of alveolar macrophages in acute lung inflammation of mice exposed to titanium dioxide nanoparticles. *Nanotoxicology* 15 (10), 1312–1330.
- Schwartz, L.A., Zurbier, C., Ince, C., 2000. Mechanical ventilation of mice. *Basic Res. Cardiol.* 95, 510–520.
- Spaan, S., Doekes, G., Heederik, D., Thorne, P.S., Wouters, I.M., 2008. Effect of extraction and assay media on analysis of airborne endotoxin. *Appl. Environ. Microbiol.* 74 (12), 3804–3811.
- Tao, S., Xu, Y., Chen, M., et al., 2021. Exposure to different fractions of diesel exhaust PM<sub>2.5</sub> induces different levels of pulmonary inflammation and acute phase response. *Ecotoxicol. Environ. Saf.* 210, 111871.
- Tsujikawa, T., Kumar, S., Borkar, R.N., et al., 2017. Quantitative multiplex immunohistochemistry reveals myeloid-inflamed tumor-immune complexity associated with poor prognosis. *Cell Rep.* 19 (1), 203–217.
- Valderrama, A., Ortiz-Hernández, P., Agraz-Cibrián, J.M., et al., 2022. Particulate matter (PM<sub>10</sub>) induces in vitro activation of human neutrophils, and lung histopathological alterations in a mouse model. *Sci. Rep.* 12 (1), 7581.
- Wang, M., Li, J., Dong, S., et al., 2020. Silica nanoparticles induce lung inflammation in mice via ROS/PARP/TRPM2 signaling-mediated lysosome impairment and autophagy dysfunction. *Part. Fibre Toxicol.* 17 (1), 1–22.
- Wang, R., Xiao, H., Guo, R., Li, Y., Shen, B., 2015. The role of C5a in acute lung injury induced by highly pathogenic viral infections. *Emerg. Microbes Infect.* 4 (1), 1–7.
- Woodruff, T.M., Nandakumar, K.S., Tedesco, F., 2011. Inhibiting the C5–C5a receptor axis. *Mol. Immunol.* 48 (14), 1631–1642.

- Yang, J., Ramirez Moral, I., van't Veer, C., et al., 2019. Complement factor C5 inhibition reduces type 2 responses without affecting group 2 innate lymphoid cells in a house dust mite induced murine asthma model. *Respir. Res.* 20 (1), 1–10.
- Yang, L., Li, C., Tang, X., 2020. The impact of PM2.5 on the host defense of respiratory system. *Front. Cell Dev. Biol.* 8, 91.
- Yang, T., Chen, R., Gu, X., et al., 2021. Association of fine particulate matter air pollution and its constituents with lung function: the China pulmonary health study. *Environ. Int.* 156, 106707.
- Yoshida, S., Hiyoshi, K., Ichinose, T., et al., 2009. Effect of nanoparticles on the male reproductive system of mice. *Int. J. Androl.* 32 (4), 337–342.
- Zaynagetdinov, R., Sherrill, T.P., Kendall, P.L., et al., 2013. Identification of myeloid cell subsets in murine lungs using flow cytometry. *Am. J. Respir. Cell Mol. Biol.* 49 (2), 180–189.
- Zhang, F., Yang, B., Wang, Y., et al., 2020. Time-and dose-resolved proteome of PM2.5-exposure-induced lung injury and repair in rats. *J. Proteome Res.* 19 (8), 3162–3175.
- Zhang, Q., Jiang, X., Tong, D., et al., 2017. Transboundary health impacts of transported global air pollution and international trade. *Nature* 543 (7647), 705–709.
- Zhao, C., Pu, W., Wazir, J., et al., 2022. Long-term exposure to PM2.5 aggravates pulmonary fibrosis and acute lung injury by disrupting Nrf2-mediated antioxidant function. *Environ. Pollut.* 313, 120017.